Annals of Nuclear Energy 132 (2019) 249–257

Contents lists available at ScienceDirect

Annals of Nuclear Energy

journal homepage: www.elsevier.com/locate/anucene

# Coupling RMC and CFD for simulation of transients in TREAT reactor

Junjie Rao, Xiaotong Shang, Ganglin Yu *, Kan Wang

*Department of Engineering Physics, Tsinghua University, Beijing 100084, China*

ARTICLE INFO

*Article history:*
Received 28 February 2019
Received in revised form 16 April 2019
Accepted 24 April 2019
Available online 29 April 2019

*Keywords:*
Transient
Monte Carlo
CFD
Coupling
TREAT

ABSTRACT

This paper introduces a transient-state coupling method using the Monte Carlo Code RMC (Reactor Monte Carlo Code) and the Computational Fluid Dynamic (CFD) code ANSYS FLUENT. RMC employs the Predictor-Corrector Quasi-Static (PCQS) method to solve space- and time-dependent neutron transport problems and uses the on-the-fly target motion sampling (TMS) for Doppler broadening. This method was performed for simulation of transients in the Transient Reactor Test Facility (TREAT). Time evolutions of power were reproduced and qualitative assessment of the model was performed by comparison with the measured power. This method successfully reproduced the experimental results of transients in TREAT reactor, and the deviation at peak power was less than 30%.



**Contents**



## 1. Introduction

The reactor status is the result of coupling of neutron physics, thermal hydraulics, material science and some others. And the multi-physics modeling is performed to accurately simulate the dynamic behavior in a reactor. One of the significant multi-physics coupling is between neutronics and thermal-hydraulics (Henry et al., 2018). As in many transients, the temperature and density of materials change, which impacts the neutron spectrum and alters the fission rate. These effects make a difference to core's behavior and inherent safety of the reactor.

Generally, there are two ways to perform the coupling. One is internal coupling and the other is external coupling. In internal coupling, the neutron transport and thermal-hydraulics are determined simultaneously and the message transfer efficiency is high,

* Corresponding author.
*E-mail address:* yuganglin@mail.tsinghua.edu.cn (G. Yu).

https://doi.org/10.1016/j.anucene.2019.04.039
0306-4549/

but the number of equations to be solved could be excessively large and it is difficult to solve these equations. As for external coupling, a script code is used for combining neutronics code and thermal-hydraulics code. The main function of the script code is exchange of the data between the codes. The advantage of external coupling is to make full use of the mature thermal-hydraulics codes.

With the rapid development of the supercomputer and the requirement of accurate three dimensional modeling of new complex reactors, Monte Carlo method plays a more and more important role in reactor analysis. Monte Carlo method can handle complex problems of continuous energy and complicated geometry. RMC is a 3-D continuous energy Monte Carlo code developed by REAL team at Tsinghua University (Wang et al., 2015). Recently, Li et al. (2012) coupled RMC and CFX to analyze the steady-state of a Pebble Bed-Advanced High Temperature Reactor (PB-AHTR). More recently, Guo et al. (2017) used RMC and COBRA-TF to simulate the steady-state of the Benchmark for Evaluation And Validation of Reactor Simulations (BEAVRS). And Guo et al. (2018) further improved the versatility and stabilization of the coupling between RMC and CTF. Most of the existing studies focused on steady-state analyses. Coupling of TRIPOLI and CFX codes was performed for steady-state operation of TRIGA research reactor by Henry et al. (2017). And Henry et al. (2018) also coupled TRIPOLI/CFX to simulate the dynamic behavior of TRIGA reactor after a control rod extraction.

We have decided to couple RMC with a computational fluid dynamic (CFD) code, ANSYS FLUENT. The reason why we chose Fluent is the relatively simple geometry of the TREAT reactor core and the reflector and the accuracy of results obtained by FLUENT. In this paper, we introduce a transient-state coupling method using RMC and FLUENT. This method was performed to simulate transients in TREAT reactor. The calculations are compared against the measured power. The Predictor-Corrector Quasi-Static (PCQS) method is described first, then the coupled calculation method is introduced in detail. After an overview of the TREAT design and its transients, the computational models of TREAT are presented in detail. Finally, the coupled calculation results are exhibited and compared with the experiments.

## 2. Predictor-corrector quasi-static (PCQS) method

The quasi static method factorizes the neutron angular flux into the amplitude function which can be transformed to the point kinetics equations and the shape function. The amplitude function changes rapidly with time and has to be solved with micro time steps while the shape function changes slower and can be solved with macro time steps. The quasi static method is widely used in deterministic methods and was first realized in multi-group Monte Carlo code TDKENO (Waddell et al., 1993). The Monte Carlo quasi static method was then improved by handling the change of the shape function called the Improved Quasi Static (IQS) method and was implemented in TDKENO-M (Bentley et al., 1996) which is a modified version of TDKENO. Yun et al. (2008) also worked on the quasi static method and compared the results with the SN method. The predictor-corrector quasi-static method was first introduced into deterministic calculation (Dulla et al., 2008) and then studied for MC calculation (Hackemack et al., 2013). Compared to the improved quasi-static method, the predictor-corrector quasi-static method shows a prompt responses of the power prediction and does not require iterations between the solution of point kinetics equation and the shape function calculation. The predictor-corrector quasi-static method was implemented in RMC by Xu et al. (2014) in a full Monte Carlo way.

To accurately describe the dynamic behavior of the neutron flux in the whole reactor core, we start from the time dependent neutron transport equation and the delayed neutron precursors equations without external neutron source:

$$\frac{1}{v}\frac{\partial\Phi(r,\Omega,E,t)}{\partial t}+L\Phi(r,\Omega,E,t)+T\Phi(r,\Omega,E,t) = S\Phi(r,\Omega,E,t)+\frac{\chi_p(E)}{4\pi}(1-\beta)F\Phi(r,\Omega,E,t)+\sum_{i=1}^{d}\frac{\chi_i(E)}{4\pi}\lambda_i C_i(r,t) \tag{1}$$

$$\frac{\partial C_i(r,t)}{\partial t}=\beta_i F\Phi(r,\Omega,E,t)-\lambda_i C_i(r,t) \tag{2}$$

where

$$L\Phi(r,\Omega,E,t)=\Omega\cdot\nabla\Phi(r,\Omega,E,t) \tag{3}$$

$$T\Phi(r,\Omega,E,t)=\Sigma_t(r,E,t)\Phi(r,\Omega,E,t) \tag{4}$$

$$S\Phi(r,\Omega,E,t)=\iint\Sigma_s(r,\Omega\to\Omega',E\to E',t)\Phi(r,\Omega',E',t)dE'd\Omega' \tag{5}$$

$$F\Phi(r,\Omega,E,t)=\nu\Sigma_f(r,E,t)\Phi(r,\Omega,E,t) \tag{6}$$

$$\beta=\sum_{i=1}^{d}\beta_i \tag{7}$$

d is the total group number of the delayed neutron precursors, $\lambda_i$ is the decay constant of the $i_{\text{th}}$ group delayed neutron precursor and $\beta_i$ is the fraction of the $i_{\text{th}}$ group delayed neutrons.

### 2.1. Point kinetics equations

In quasi-static method, the neutron angular flux is factorized into the amplitude function $T(t)$ and the shape function $\Psi(r,\Omega,E,t)$ as

$$\Phi(r,\Omega,E,t)=\Psi(r,\Omega,E,t)T(t) \tag{8}$$

Then Eq. (8) is substituted into Eq. (1), and Eq. (1) is then divided by $T(t)$ to yield the following equation:

$$\frac{1}{v}\frac{\partial\Psi(r,\Omega,E,t)}{\partial t}+\frac{1}{vT(t)}\frac{dT(t)}{dt}\Psi(r,\Omega,E,t)+L\Psi(r,\Omega,E,t)+T\Psi(r,\Omega,E,t) = S\Psi(r,\Omega,E,t)+\frac{\chi_p(E)}{4\pi}(1-\beta)F\Psi(r,\Omega,E,t)+\frac{1}{T(t)}\sum_{i=1}^{d}\frac{\chi_i(E)}{4\pi}\lambda_i C_i(r,t) \tag{9}$$

We integrate Eq. (9) over the space $r$, energy $E$ and angle $\Omega$ and introduce the normalization condition:

$$\iiint\frac{1}{v}\Psi(r,\Omega,E,t)W(r,\Omega,E)dVdEd\Omega=constant \tag{10}$$

where $W(r,\Omega,E)$ is the weighting function. According to the reference (Shang et al. 2018), the initial adjoint flux is better as the weighting function than a constant value. In our work, we chose the initial adjoint flux as the weighting function.

The Eqs. (10) and (2) can be rewritten as

$$\frac{dT(t)}{dt}=\frac{\rho(t)-\bar{\beta}(t)}{\Lambda(t)}T(t)+\sum_{i=1}^{d}\lambda_i c_i(t) \tag{11}$$

$$\frac{\partial c_i(t)}{\partial t}=\frac{\bar{\beta}_i(t)}{\Lambda(t)}T(t)-\lambda_i c_i(t) \tag{12}$$

where

$$F(t)=\iiint dVd\Omega dEW(r,\Omega,E)\frac{\chi_p(E)}{4\pi}\iiint d\Omega' dE' F\Psi(r,\Omega',E',t) \tag{13}$$

$$\Lambda(t)=\frac{1}{F(t)}\left\langle\frac{\Psi(r,\Omega,E,t)}{v},W(r,\Omega,E)\right\rangle \tag{14}$$

$$\rho(t)=\frac{\left\langle\frac{\chi_p(E)}{4\pi}F\Psi(r,\Omega,E,t)-L\Psi(r,\Omega,E,t)-T\Psi(r,\Omega,E,t)+S\Psi(r,\Omega,E,t),W(r,\Omega,E)\right\rangle}{F(t)} \tag{15}$$

$$\bar{\beta}_i(t)=\frac{\left\langle\frac{\chi_p(E)}{4\pi}\beta_iF\Psi(r,\Omega,E,t),W(r,\Omega,E)\right\rangle}{F(t)} \tag{16}$$

$$c_i(t)=\frac{\left\langle\frac{\chi_i(E)}{4\pi}C_i(r,\Omega,E,t),W(r,\Omega,E)\right\rangle}{\left\langle\frac{\Psi(r,\Omega,E,t)}{v},W(r,\Omega,E)\right\rangle} \tag{17}$$

$$\bar{\beta}(t)=\sum_{i=1}^{d}\bar{\beta}_i(t) \tag{18}$$

Eqs. (11) and (12) are the point kinetics equations in the quasi-static method.

### 2.2. The fixed source Equation in PCQS method

In the PCQS method, the implicit Euler Method which is the fully backward scheme is applied for the differential treatment of the neutron flux and delayed neutron precursor concentrations:

$$\frac{\partial\Phi(t_{n+1})}{\partial t}\approx\frac{\Phi(t_{n+1})-\Phi(t_n)}{\Delta t} \tag{19}$$

$$\frac{\partial C_i(t_{n+1})}{\partial t}\approx\frac{C_i(t_{n+1})-C_i(t_n)}{\Delta t} \tag{20}$$

where $n$ donates the $n_{\text{th}}$ time step. When Eqs. (19) and (20) are substituted into Eqs. (1) and (2), Eqs. (1) and (2) can be rewritten as:

$$\begin{aligned}&L\Phi(r,\Omega,E,t_{n+1})+T'\Phi(r,\Omega,E,t_{n+1})\\&=S\Phi(r,\Omega,E,t_{n+1})+\frac{\chi_p(E)}{4\pi}(1-\beta)F\Phi(r,\Omega,E,t_{n+1})+\sum_{i=1}^{d}\\&\times\frac{\lambda_i\Delta t}{1+\lambda_i\Delta t}\frac{\chi_i(E)}{4\pi}\beta_iF\Phi(r,\Omega,E,t_{n+1})+\sum_{i=1}^{d}\frac{1}{1+\lambda_i\Delta t}\\&\times\frac{\chi_i(E)}{4\pi}\lambda_iC_i(r,t_n)+\frac{1}{v\Delta t}\Phi(r,\Omega,E,t_n)\end{aligned} \tag{21}$$

where

$$T'\Phi(r,\Omega,E,t_{n+1})=(\Sigma_t(r,E,t_{n+1})+\frac{1}{v\Delta t})\Phi(r,\Omega,E,t_{n+1}) \tag{22}$$

The predicted angular flux $\Phi^{\text{predicted}}(r,\Omega,E,t)$ can be obtained from the solution of Eq. (21) and the kinetics parameters can be estimated from Eqs. (13)–(18) by replacing the shape function $\Psi(r,\Omega,E,t)$ with the predicted angular flux $\Phi^{\text{predicted}}(r,\Omega,E,t)$ and the amplitude function $T(t)$ can be obtained from Eqs. (11) and (12). Then the corrected angular flux $\Phi^{\text{corrected}}(r,\Omega,E,t)$ can be calculated as:

$$\Phi^{corrected}(r,\Omega,E,t)=\Phi^{predicted}(r,\Omega,E,t)T(t)\frac{\left\langle\frac{\Phi(r,\Omega,E,t_0)}{v},W(r,\Omega,E)\right\rangle}{\left\langle\frac{\Phi^{predicted}(r,\Omega,E,t)}{v},W(r,\Omega,E)\right\rangle} \tag{23}$$

In Monte Carlo Code RMC, Eq. (21) is solved with modified source iteration method whose procedure is similar to that of the standard source iteration method in eigenvalue calculation but fission source neutrons are modified by the decay source neutrons and time absorption source neutrons. According to the conservation principle in the Monte Carlo solution process, weighting integration of Eq. (21) on the phase space yields:

$$\begin{aligned}&\left\langle S\left(\vec{r},\vec{\Omega},E,t_{n+1}\right),W(\vec{r},\vec{\Omega},E)\right\rangle\\&=\left\langle L\Phi\left(\vec{r},\vec{\Omega},E,t_{n+1}\right)+T'\Phi\left(\vec{r},\vec{\Omega},E,t_{n+1}\right)\right.\\&\quad\left.-S\Phi\left(\vec{r},\vec{\Omega},E,t_{n+1}\right),W(\vec{r},\vec{\Omega},E)\right\rangle\\&=\left\langle L\Phi\left(\vec{r},\vec{\Omega},E,t_{n+1}\right)+T\Phi\left(\vec{r},\vec{\Omega},E,t_{n+1}\right)\right.\\&\quad\left.-S\Phi\left(\vec{r},\vec{\Omega},E,t_{n+1}\right),W(\vec{r},\vec{\Omega},E)\right\rangle\\&\quad+\left\langle\frac{1}{v\Delta t_n}\Phi\left(\vec{r},\vec{\Omega},E,t_{n+1}\right),W(\vec{r},\vec{\Omega},E)\right\rangle\end{aligned} \tag{24}$$

Then Eq. (15) can be rewritten as

$$\rho(t)=1-\frac{\left\langle S\left(\vec{r},\vec{\Omega},E,t_{n+1}\right),W(\vec{r},\vec{\Omega},E)\right\rangle-\left\langle\frac{1}{v\Delta t_n}\Phi\left(\vec{r},\vec{\Omega},E,t_{n+1}\right),W(\vec{r},\vec{\Omega},E)\right\rangle}{F(t)} \tag{25}$$

According to Eq. (25), $\rho(t)$ can be estimated without complicated handling of the leakage, absorption or scattering term.

### 2.3. Strategy for time steps and solution of point kinetics equation

Macro and micro time step strategy is adopted in the PCQS method. The transient fixed source equation is solved and the kinetics parameters are estimated in each macro time step. Between the two macro time steps, the kinetics parameters are linearly interpolated in each micro time step. In RMC, the point kinetics equation is solved with the fourth order Runge-Kutta method (Butcher et al., 1987) which proves to have good precision when solving the ordinary differential equations.

## 3. Coupling algorithm

RMC and FLUENT are linked through a file sharing system and python script which iterates between the two codes as seen in Fig. 1. RMC communicates with FLUENT through output and input files. RMC outputs the total fission power and neutron flux for each mesh at the end of every time interval. Then the power density for

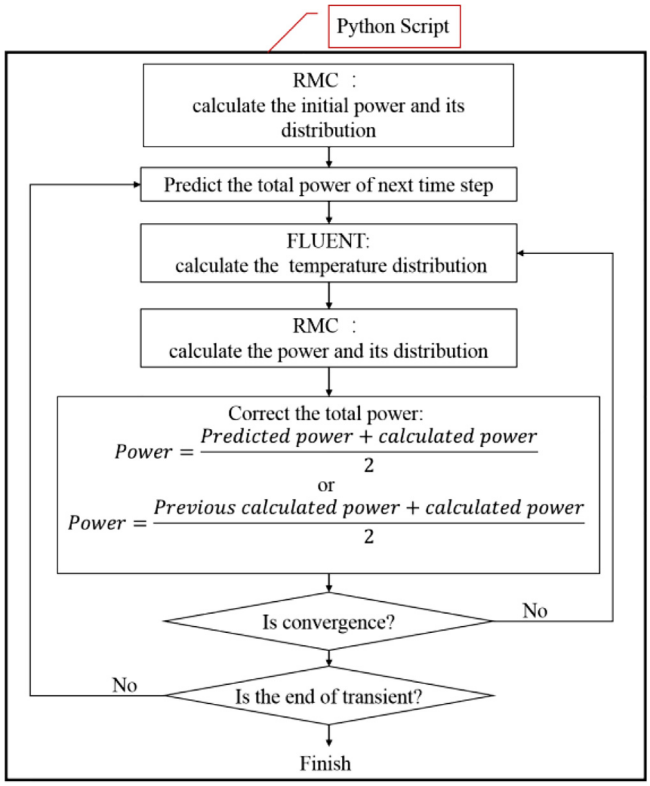


**Fig. 1.** Flow chart of coupling RMC-FLUENT system.

each mesh volume for FLUENT was obtained. When RMC has completed a calculation for a time step, RMC is paused and FLUENT starts to calculate temperature. FLUENT uses the energy source term from RMC to generate a temperature distribution. Once FLUENT has produced the temperature distribution, the python script processes the file output by FLUENT and obtains a temperature distribution read by RMC. And the python script signals RMC to continue to calculate for the next time step. RMC reads the temperature distribution and the temperatures of materials change. Based on this corrected temperature, RMC adjusts the cross sections with the on-the-fly target motion sampling (TMS) for Doppler broadening. Currently, the coupling method only supports changes in temperature. What's more, this method supports temperature changes in the form of grids or cells, which is convenient for user to use.

The detailed steps of the simulation are summarized as follows. In simulations, the idea of predictive correction is adopted. In order to save time, we chose to iterate twice and the results have approached convergence.

- Step 1. At time $t_n$, temperature and power are known. In coupled simulations, the power is assumed to be approximately exponential change in a short time. Therefore, the power $P_1$, at the end of the next time interval $t_{n+1}$, is predicted by exponential fitting with the power at the end of the previous two time intervals $t_{n-1}$ and $t_n$. The average power of the next time interval is obtained.
- Step 2. FLUENT calculates the temperature distribution at $t_{n+1}$. Then RMC calculates the power $P_2$ at $t_{n+1}$. The power $P_3$ at $t_{n+1}$, temporarily, is modified by averaging the calculated value $P_2$ and the predicted value $P_1$. The average power of the time interval between $t_n$ and $t_{n+1}$ is modified with $P_3$ and exponential fitting.
- Step 3. FLUENT recalculates the temperature distribution at $t_{n+1}$. Then RMC recalculates the power $P_4$ at $t_{n+1}$. The power $P_5$ at $t_{n+1}$, is corrected by averaging $P_3$ and $P_4$. The average power of the time interval between $t_n$ and $t_{n+1}$ is modified with $P_5$ and exponential fitting. FLUENT recalculates the corrected temperature distribution at $t_{n+1}$.

## 4. TREAT transients

From the original startup of the Transient Reactor Test (TREAT) reactor in 1959 to being placed on a nonoperational standby status in 1994, TREAT was used to perform hundreds of experiments involving power transients (Kontogeorgakos et al., 2013). TREAT is a high-enriched, homogeneous fueled reactor which is air cooled, graphite moderated, and graphite reflected. It was designed, built, and operated in a manner to allow a wide range of fueled test samples to be placed in the core and be subject to a wide variety of power transients. All experiments showed that strict TREAT core temperature limits would not be exceeded, even in the event of a prompt supercritical accident.

There are a variety of core assemblies so that TREAT can be configured into several configurations of varying types and number of core assemblies. The maximum TREAT consists of 19*19 assemblies and its active core is 193.04 cm square and 121.92 cm high. The UO2 fuel, enriched to 93.1 wt%, is finely dispersed in a graphite matrix. And the ratio of $^{235}U$ to graphite is approximately 1:10,000.

The M8 calibration experiment was a series of 23 irradiations in TREAT planned to provide the essential calibration information specifically needed for planning and analysis of the M8 test to be performed in the post-upgrade TREAT core (Robinson et al., 1994). There are 20 control rod fuel assemblies in TREAT and they are divided into three groups: 4 compensation rods, 8 control/shutdown rods, 8 transient rods. Temperature-limited transients (Transients 2855, 2856 and 2857) were generated by computer-controlled sudden withdrawals of transient rods with typical time durations of several hundred milliseconds (Kontogeorgakos et al., 2013). Temperature-limited transients define the maximum reactivity of the core and establish limiting safety system settings and safety limits for the core loading. For transient 2855, 2856 and 2857, this rod withdrawal was the equivalent of 1,800, 3,000 and 3,850 pcm of reactivity insertion, respectively. And power rises were terminated by temperature feedback. Table 1 presents the details of temperature-limited transients (Robinson et al., 1994).

## 5. Computational models

### 5.1. Neutron physics model

The neutron transport simulations were performed with RMC. The cross sectional and side views of computational model are presented in Fig. 2. The fuel was surrounded by 60.96 cm graphite

**Table 1**
Temperature limited transients.

| Transients | Nominal Reactivity | Nominal Energy (MJ) | Compensation Rods (in) | Control/Shutdown Rods (in) | Transient Rods (in) | Initial Core Temperature (°C) |
|---|---|---|---|---|---|---|
| 2855 | 1.8% | 792 | 58.5 | 28.72 | 26.5 | 26 |
| 2856 | 3% | 1,572 | 58.5 | 33.05 | 21.5 | 24 |
| 2857 | 3.85% | 2,265 | 58.5 | 36.40 | 18.5 | 25 |

reflectors on the top, bottom and all sides of the core. The active core and the graphite reflectors were explicitly modeled. In addition, the rest of TREAT which had a negligible impact on the behavior of neutrons in the core wasn't taken into account to save computational time. In this simulation, only temperature was corrected, and material density was considered constant because there is no need to change material density for a solid fuel during a short transient (Sorrell et al., 2018). The active core was divided into 19*19*20 grids in length, width and height.

As shown in Table 1, the initial core temperature was about 298 K. However, due to the lack of 298 K nuclear data, the initial core temperature was set to 300 K in simulations. The ENDF/B-VII.0 nuclear data set was used for neutron physics calculations.

### 5.2. Thermal-hydraulics model

The CFD simulations were performed with the commercial code ANSYS FLUENT. Only active core, top and bottom graphite reflectors were taken into account to save the computational time. Meanwhile, the void, the Zircaloy-3 cladding encasing fuel and 6063-aluminum encasing graphite reflectors were substituted by the fuel. All temperature boundary conditions were defined as convective heat transfer boundary conditions and the heat transfer coefficient is 10 $W/(m^2\hat{A}\cdot K)$. According to our studies, the heat transfer coefficient varying within a small range from 10 to 24 $W/(m^2\hat{A}\cdot K)$ has a negligible impact. The thermal conductivity of graphite-urania for TREAT fuel and specific heat of TREAT fuel specimen were given (Handwerk et al., 1960). The formulas were obtained with the curves. The formulas for thermal conductivity and specific heat as a function of temperature are as follows.

$$k = 8.36 \times 10^{-6} t^2 - 0.01886t + 27.804 \tag{26}$$

$$C = \begin{cases} -0.0098936t^2 + 10.619t - 1611.4 & t \le 573.15 \\ 1224.8 & t > 573.15 \end{cases} \tag{27}$$

where $k$ is the thermal conductivity of fuel, $t$ is the temperature of fuel in unit of K, $C$ is the specific heat of fuel.

## 6. Results

Temperature-limited transients (Transients 2855, 2856 and 2857) were generated by computer-controlled sudden withdrawals of transient rods with typical time durations of several hundred milliseconds (Kontogeorgakos et al., 2013). For transient 2855, 2856 and 2857, transient rods withdrawal was equivalent to 1,800, 3,000 and 3,850 pcm of reactivity insertion, respectively. In the simulations, RMC computations were done with 300 cycles of 100,000 neutrons. All the simulations of three transients were performed on a computer with 32 cores (two processors Intel(R) Xeon(R) Gold 6130 CPU at 2.10 GHz of 16 cores) and 64 GB DDR4 memory. And RMC used 48 processes and FLUENT used one process. It took about 84 h for the simulation of a transient, most of which was used by RMC.

### 6.1. Transient 2855

For transient 2855, the sudden withdrawal of transient rods was the equivalent of 1,800 pcm of reactivity insertion. Due to the temperature feedback, the reactor reached a new critical state and then became subcritical. Fig. 3 shows the result of the coupling calculation and experiment. The result of the experiment is from Mausolff et al. (2018). The peak power of the experiment is 1,293 MW while that of the coupling calculations is 1,557 MW, which differs from experiment by 20%. The point kinetics refers to using the point kinetics method and an empirical relation for total energy and reactivity feedback from experimental TREAT data (Kontogeorgakos et al., 2013) to simulate transients. The result calculated with point kinetics and the details of the point kinetics method can be found in Rao et al. (2018). Table 2 presents the flux update times.

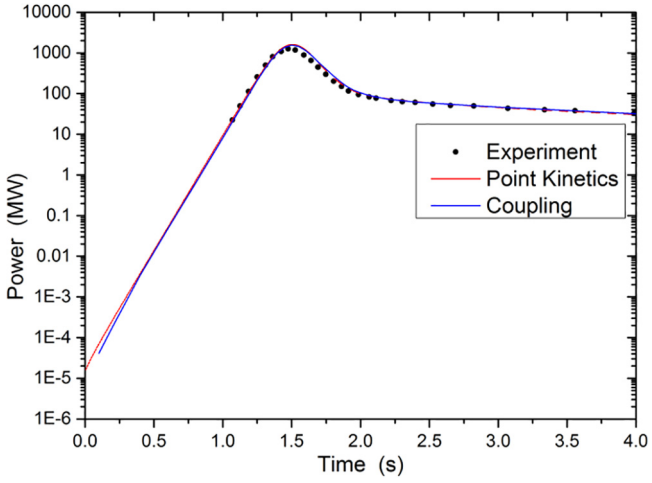


**Fig. 3.** Calculated integral power as a function of time for transient 2855.

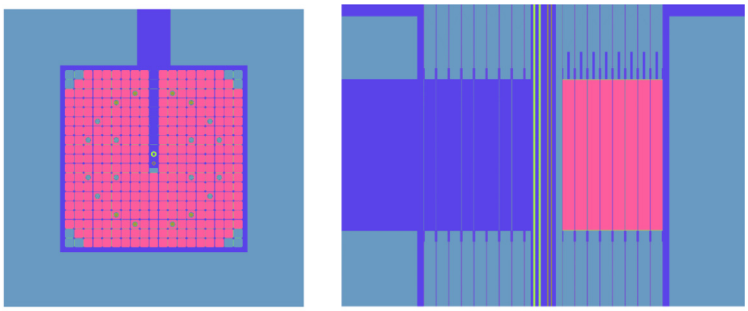

( Graphite Reflector, Air, Fuel Assembly, Control Assembly)

**Fig. 2.** TREAT cross sectional and side views of half slotted M8 core configuration. (Kontogeorgakos et al., 2013; John and Mark, 2015) ( Graphite Reflector, Air, Fuel Assembly, Control Assembly).

**Table 2**
Flux update times for transient 2855.

| | |
|---|---|
| Flux shapes | 33 |
| Flux update times[s] | 0.0,0.1,0.2,0.4,0.6,0.8,1.0,1.1,1.2,1.25,1.3,1.35,1.4,1.45,1.5,1.55,1.6,1.65,1.7,1.75,1.8,1.85,1.9,1.95,2.0,2.05,2.1,2.2,2.4,2.7,3.0,4.0,60 |

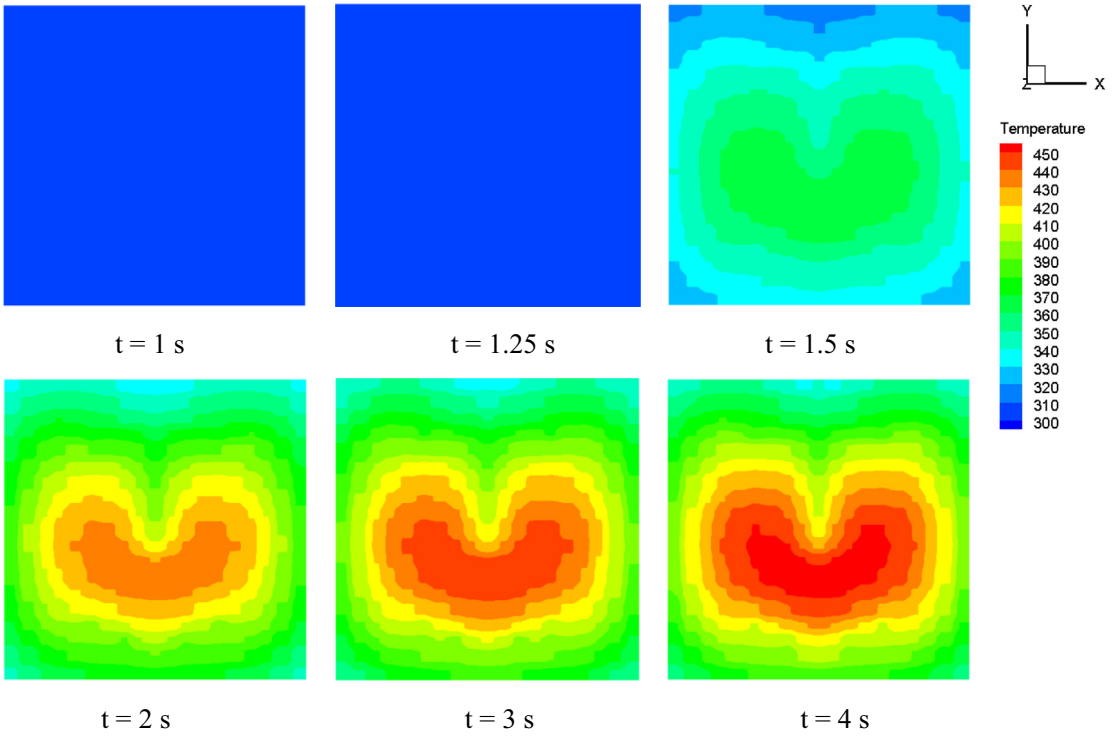


**Fig. 4.** Fuel temperature distributions of the middle slice in axial direction for transient 2855.

The resulting temperature distribution of the graphite-fuel matrix takes the form seen in Fig. 4, which displays the temperature distributions of the middle slice in axial direction throughout time in the simulation. Fig. 5 presents the reactivity and average temperature of the reactor. Before 1.25 s, temperature changes slowly. Then temperature starts to increase quickly. When the power reaches the maximum, the average temperature is about 345 K.

As shown in Fig. 5, the curve of the reactivity varying with time is not smooth. In this simulation, the number of neutrons used per cycle was 100,000 and the standard deviation of the reactivity was 30 pcm, which may have an impact on the power. To simplify the thermal-hydraulics model and save the computational time, we only considered the fuel and top and bottom reflectors. That is, the zone of thermal-hydraulics model consists of three parts: the top reflector, the fuel and the bottom reflector. The cladding and

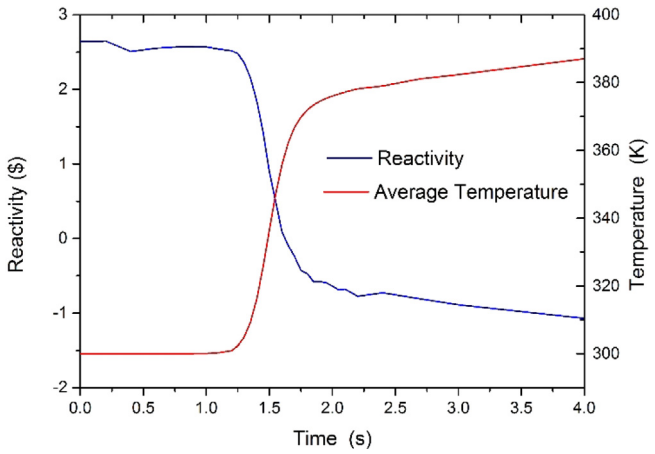


**Fig. 5.** Calculated reactivity and average temperature of the system for transient 2855.

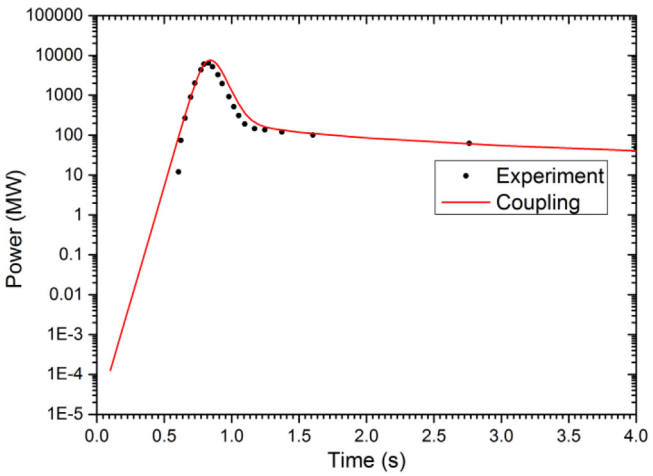


**Fig. 6.** Calculated integral power as a function of time for transient 2856.

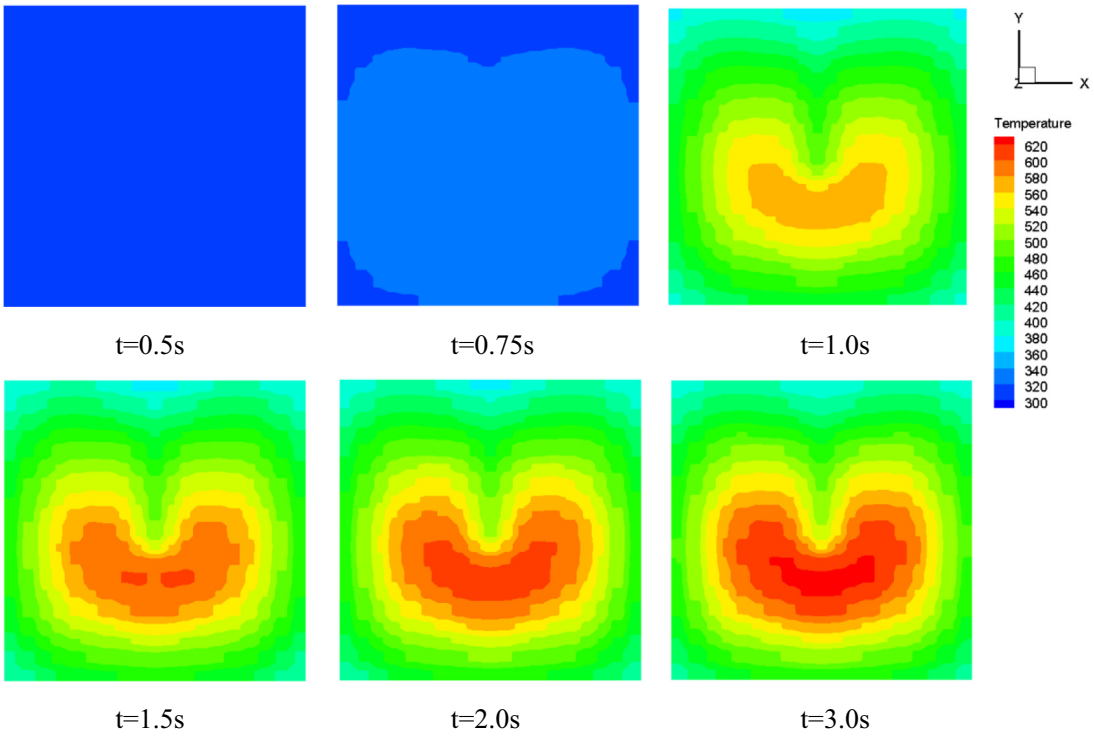


**Fig. 7.** Fuel temperature distributions of the middle slice in axial direction for transient 2856.

interspace were replaced by fuel, which caused the heat transfer properties to differ from the actual ones. The temperature distribution, calculated reactivity and power may be also influenced.

### 6.2. Transient 2856

For transient 2856, the sudden reactivity insertion was 3,000 pcm. Due to the higher reactivity, the time for updating a shape was smaller than the previous simulation. Fig. 6 shows the result of the coupling calculation and the experiment. The peak power of the experiment is 6,260 MW while that of the coupling calculations is 7,576 MW. The difference between the two is 21%. As with the previous simulation, the calculated power near the peak is higher than the measured value. Fig. 7 presents the resulting temperature distribution of the graphite-fuel matrix. The reactivity and average temperature of the reactor for transient 2856 are given in Fig. 8. Table 3 presents the flux update times.

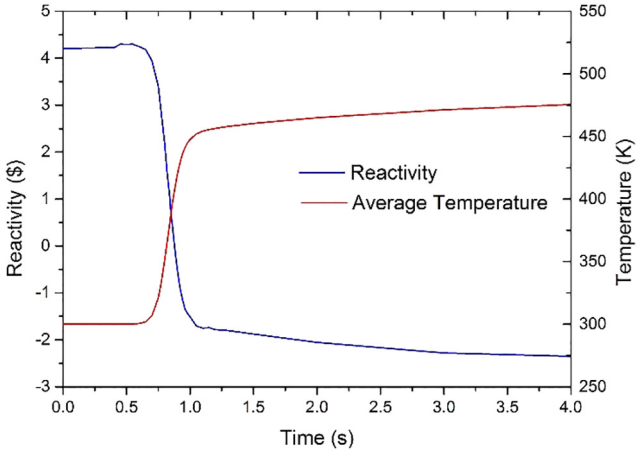


**Fig. 8.** Calculated reactivity and average temperature of the system for transient 2856.

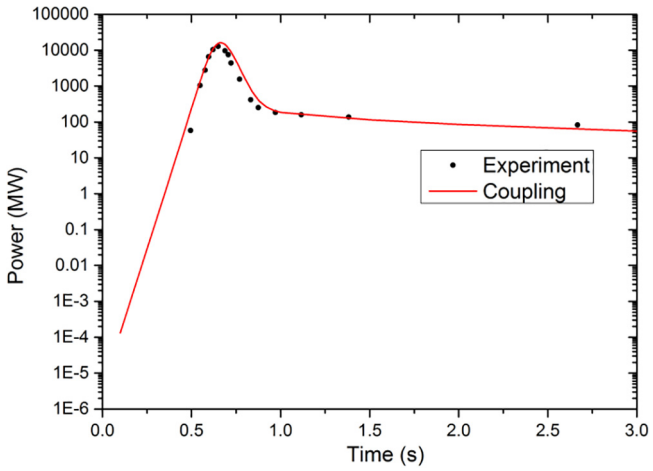


**Fig. 9.** Calculated integral power as a function of time for transient 2857.

**Table 3**
Flux update times for transient 2856.

| Flux shapes | 37 |
|---|---|
| Flux update times[s] | 0.0,0.1,0.2,0.3,0.4,0.45,0.5,0.55,0.6,0.65,0.7,0.75,0.775,0.8,0.82,0.84,0.85,0.86,0.88,0.9,0.92,0.94,0.95,0.96,0.98,1.0,1.05,1.1,1.15,1.2,1.25, 1.3,1.5,2.0,3.0,4.0,60 |

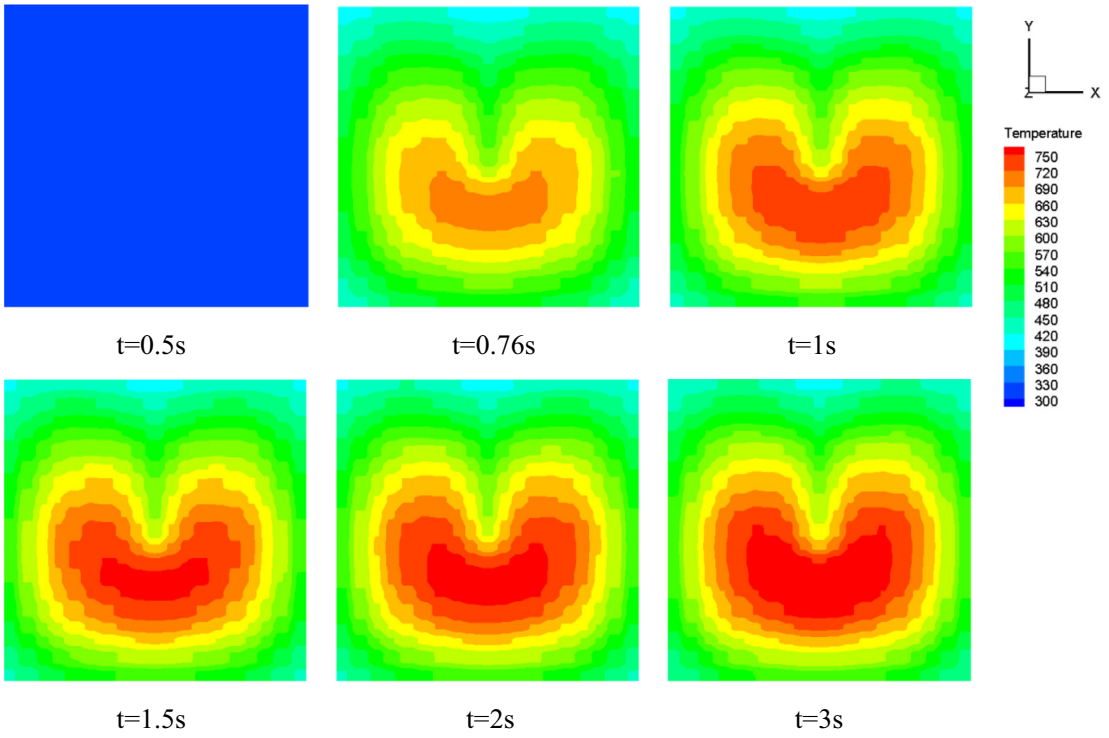


**Fig. 10.** Fuel temperature distributions of the middle slice in axial direction for transient 2857.

### 6.3. Transient 2857

For transient 2857, the sudden withdrawal of transient rods was the equivalent of 3,850 pcm of reactivity insertion. Fig. 9 shows the result of the coupling calculation and experiment. The peak power of the experiment is 12,645 MW while that of the coupling calculations is 16,208 MW. The difference between the two is 28%. As with the previous two simulations, the calculated power near the peak is higher than the measured value. Fig. 10 presents the resulting temperature distribution of the graphite-fuel matrix. The reactivity and average temperature of the reactor for transient 2857 are given in Fig. 11. Table 4 presents the flux update times.

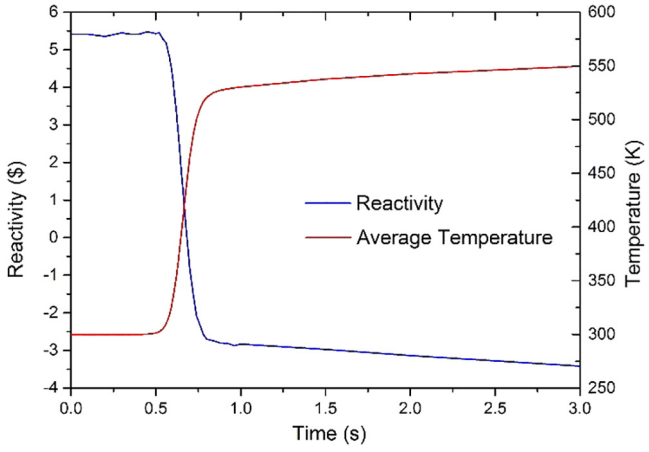


**Fig. 11.** Calculated reactivity and average temperature of the system for transient 2857.

## 7. Conclusions

A transient-state coupling method using RMC/FLUENT was proposed for calculating feedback effects in a transient simulation. In this coupled system, the predictor-corrector quasi-static method was used to tackle the neutron kinetics in RMC and the thermal-hydraulics was calculated through FLUENT. This coupling multi-physics method was applied to reproduce TREAT reactor behaviour in time for short transients where the sudden reactivity was 2.5–5.4 dollars. Calculated results were compared with power measured during temperature limited transients, and the deviation at peak power was less than 30%.

## Acknowledgement

This work was partially supported by the National Natural Science Foundation of China [grant number 11775127] and Science and Technology on Reactor System Design Technology Laboratory.

**Table 4**
Flux update times for transient 2857.

| | |
|---|---|
| Flux shapes | 40 |
| Flux update times[s] | 0.0,0.1,0.2,0.3,0.35,0.4,0.45,0.5,0.52,0.54,0.56,0.57,0.58,0.59,0.6,0.61,0.62,0.63,0.64,0.65,0.66,0.67,0.68,0.69,0.7,0.72,0.74,0.76,0.78,0.8,0.84,0.88, 0.92,0.96,1.0,1.5,2.0,3.0,4.0,60 |

## References


Bentley, C.L., 1996. Improvements in a hybrid stochastic/deterministic method for transient three-dimensional neutron transport. Ph. D. Dissertation, University of Tennessee.

Butcher, J.C., 1987. The Numerical Analysis of Ordinary Differential Equations: Runge-Kutta and General Linear Method. Wiley, Chichester and New York.

Dulla, S., Mund, Ernest H., Piero, R., 2008. The quasi-static method revisited. Prog. Nucl. Energy 50 (8), 908–920.

Guo, J.J., Liu, S.C., Shang, X.T., Huang, S.F., Wang, K., 2017. Coupled neutronics/thermal-hydraulics analysis of a full PWR core using RMC and CTF. Ann. Nucl. Energy 109, 327–336.

Guo, J.J., Liu, S.C., Shang, X.T., Shen, Q.C., Guo, X.Y., Huang, S.F., Wang, K., Chai, X. M., 2018. Versatility and stabilization improvements of full core neutronics/thermalhydraulics coupling between RMC and CTF. Nucl. Eng. Des. 332, 88–98.

Hackemack, M.W. et al., 2013. A Monte Carlo Implementation of the Predictor-Corrector Quasi-Static Method. Proceedings of the International Conference Mathematics and Computational Methods Applied to Nuclear Science and Engineering (M&C 2013), Sun Valley, Idaho (United States).

Handwerk, J.H., Lied, R.C., 1960. The Manufacture of the Graphite-Urania Fuel Matrix for TREAT. ANL-5963, Argonne National Laboratory, Lemont, Illinois (United States).

Henry, R., Tiselj, I., Snoj, L., 2017. CFD/Monte-Carlo neutron transport coupling scheme, application to TRIGA reactor. Ann. Nucl. Energy 110, 36–47.

Henry, R., Tiselj, I., Snoj, L., 2018. Transient CFD/Monte-Carlo neutron transport coupling scheme for simulation of a control rod extraction in TRIGA reactor. Nucl. Eng. Des. 331, 302–312.

John, D.B., Mark, D.D., 2015. Baseline Assessment of TREAT for Modeling and Analysis Needs. INL/EXT-15-35372, Idaho National Laboratory, Idaho Falls, Idaho (United States).

Kontogeorgakos, D., Derstine, K., Wright, A., Bauer, T., Stevens, J., 2013. Initial neutronics analyses for HEU to LEU fuel conversion of the Transient Reactor Test Facility (TREAT) at the Idaho National Laboratory. Technical Report ANL/GTRI/TM–13/4. Argonne National Laboratory, Lemont, IL (United States).

Li, L.S., Yuan, H.M., Wang, K., 2012. Coupling of RMC and CFX for analysis of pebble bed-advanced high temperature reactor core. Nucl. Eng. Des. 250, 385–391.

Mausolff, Z., DeHart, M., Goluoglu, S., 2018. Enhanced geometric capabilities for the transient analysis code T-ReX and its application to simulating TREAT experiments. Prog. Nucl. Energy 105, 236–246.

Rao, J.J., Shang, X.T., Wang, K., 2018. Verification of transient analysis capability of RMC with TREAT temperature limited transients from M8 calibration experiments. Transactions of the American Nuclear Society, Vol. 119, 1313, Orlando, Florida, November 11–15, 2018.

Robinson, W.R., Bauer, T.H., May 1994. The M8 Power Calibration Experiment (M8CAL). Technical Report ANL-IFR–232. Argonne National Laboratory, Lemont, IL (United States).

Shang, X.T., Shi, G.L., Wang, K., 2018. One step method for multigroup adjoint neutron flux through continuous energy Monte Carlo calculation. Proceedings of the 2018 26th International Conference on Nuclear Engineering (ICONE26), London, England, July 22-26, 2018.

Sorrell, N.C., Hawari, A.I., 2018. TREAT M2 experiment modeling for transient benchmark analysis. Proceedings of the International Conference on the Physics of Reactors (PHYSOR-2018), Cancun, Mexico, April 22-26, 2018.

Waddell, M.W., Jr., Dodds, H. L., 1993. A method for transient, three-dimensional neutron transport calculations. Proceedings of the Topical Meeting on Mathematics and Computation, 633, Karlsruhe, Germany, April 19–23, 1993.

Wang, K. et al., 2015. RMC – A Monte Carlo code for reactor core analysis. Ann. Nucl. Energy 82, 121–129.

Xu, Q., Wang, K., 2014. Development of quasi-static dynamic simulation capability in Monte Carlo Code RMC. Transactions of the American Nuclear Society, Vol. 110, 231, Anaheim, CA, November 9-13, 2014.

Yun, S., Kim, J.W., Cho, N.Z., 2008. Monte Carlo space-time reactor kinetics method and its verification with time-dependent SN method. Proceedings of the International Conference on the Physics of Reactors (PHYSOR-2008), Interlaken, Switzerland, September 14-19, 2008.